# Doubling of Block Copolymer Line Patterns by Electron-Beam-Fabricated Templates

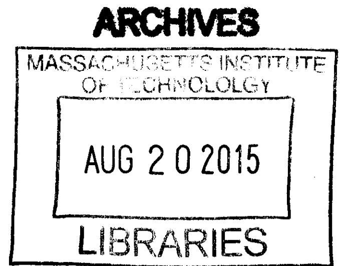


by Kameron L. Oser

B.S. Electrical Science and Engineering

Massachusetts Institute of Technology, 2013

Submitted to the
Department of Electrical Engineering and Computer Science
in Partial Fulfillment of the Requirements for the Degree of

Master of Engineering in Electrical Science and Engineering

at the

Massachusetts Institute of Technology

September 2014 [February 2015]

Copyright 2014 Kameron L. Oser. All rights reserved.

The author hereby grants to M.I.T. permission to reproduce and to distribute publicly paper and electronic copies of this thesis document in whole and in part in any medium now known or hereafter created.

Author: Signature redacted

Department of Electrical Engineering and Computer Science
September 26, 2014

Certified by: Signature redacted

Karl K. Berggren
Professor of Electrical Engineering
September 26, 2014

Accepted by: Signature redacted

Albert R. Meyer
Chairman, Master of Engineering Thesis Committee

Doubling of Block Copolymer Line Patterns by Electron-Beam-Fabricated Templates

by Kameron L. Oser

Submitted to the Department of Electrical Engineering and Computer Science

September 26, 2014

In Partial Fulfillment of the Requirements for the Degree of Master of Engineering in Electrical Science and Engineering

## Abstract

The doubling of block copolymer (BCP) line patterns by electron-beam-fabricated template patterns is presented. Difficulties in achieving low defect self-assembly within the narrow line patterns are discussed. To address these issues, experimental approaches were investigated of narrowing the polymer's minority block through solvent annealing, and adjusting length of the polymer brush responsible for functionalizing the template lines. While narrowed polymer lines were not achieved through solvent annealing, low defect self-assembly of BCP within doubling template patterns was achieved by utilizing a polymer brush of high molecular weight (28 kg $mol^{-1}$).

# Chapter 1

# Introduction

This chapter introduces the concepts of block copolymer self-assembly, electron-beam lithography, and the combination of these technologies for achieving high-density nanopatterns.

## 1.1 Block Copolymer Self-Assembly

Block copolymers (BCPs) are a class of polymer possessing a unique structure which enables self-assembly of nanoscale structures.[1,2] Each BCP molecule is composed of distinct polymer chains, or blocks, which are covalently bonded. BCPs can be composed of many blocks in various arrangements, such as linear chains or stemming from a central bond in a star-like arrangement.[2–4] This work however, exclusively investigates the case of a linear chain of only two blocks, as shown in Figure 1.1, for its simplicity and ease of control in comparison to more complex BCPs. As such, explanation will be given in the context of these simpler BCPs. Self-assembly is driven by immiscibility between the two BCP blocks, which cannot separate over longer distances due to their covalent bond. BCPs are

therefore driven to arrange in configurations which geometrically group the similar blocks from each BCP molecule. Length scales of geometries resulting from this microphase separation are thus closely related to the polymer chain length[2]. These concepts are illustrated in Figure 1.1.

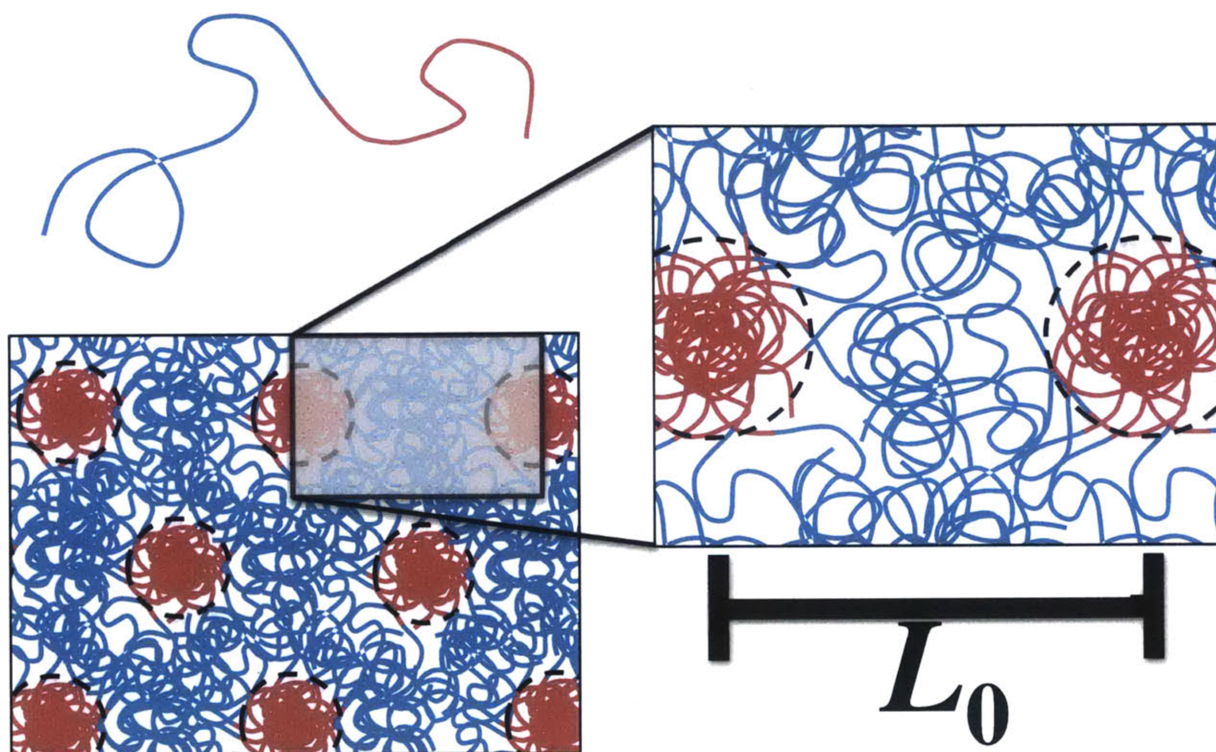


**Figure 1.1** An cartoon illustration of BCPs. The lone two-color line at the top represents a diblock copolymer. The differing color represents the differnet material for each block. For self-assembly, these blocks are highly immiscible but unable to separate over long distances due to the covalent bond connecting them. An cartoon example of spherical self-assembly is shown in the lower image, and the closer zoom up illustrates how the distance between microdomains depends heavily on the length of the BCP.

BCPs can self-assemble into various morphologies, governed by many parameters. Segregation strength is one such parameter, mentioned above, and can be quantified by the parameter $\chi N$, where $\chi$ is the Flory-Huggins interaction parameter, describing the incompatibility between blocks, and $N$ is the degree of polymerization.[1,2] Another critical parameter is each block's fraction of the total chain length, generally discussed as a volume fraction. The combination the parameters $\chi N$ and volume fraction is important for determining what morphology results from self-assembly. The general effect of these parameters on morphology of diblock copolymers is presented in the phase diagram in Figure 1.2, which was reproduced from reference 2. As indicated above, a reasonable $\chi N$ is required for driving self-assembly. For the BCP to exit the disordered phase and self-assemble, the theoretical $\chi N$ is required to be greater than 10.5.[1] As the effective volume fraction of each block is changed, the microdomains for each block change in size until the BCP morphology is pushed into a neighboring phase. For example, a BCP in the cylindrical phase, with decreasing volume fraction of the current minority block, will experience some combination of a decrease in cylindrical diameter and an increase pitch, the distance between these microdomains, until the minority block transitions to a spherical morphology.

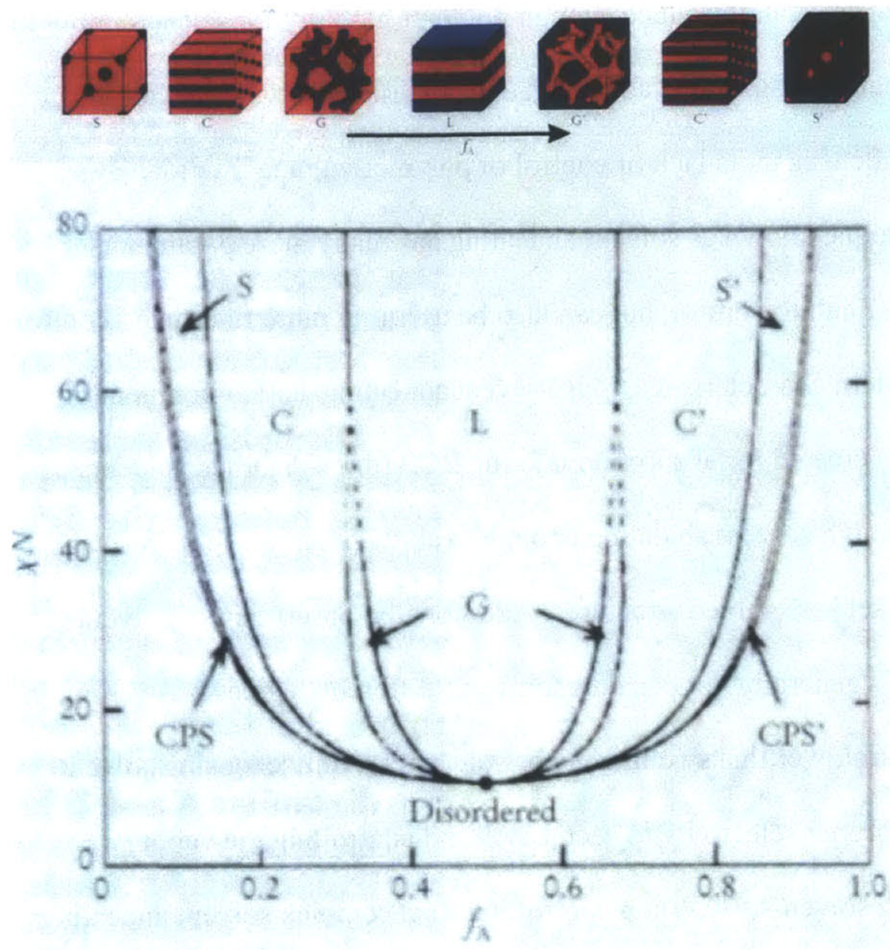


**Figure 1.2** The general phase diagram for diblock copolymers reproduced from reference 2. The phase diagram shows the a minimum $\chi N$ is necessary ordered morphology to occur. The volume fration, in this figure $f_A$, strongly controls the assembled morphology.

The environment in which the BCP anneals also plays a critical role in determining final morphology. Introducing heat to the BCPs under vacuum[5] or

nitrogen atmosphere[6] can introduce enough polymer mobility for self-assembly to occur. Thermal annealing can be advantageous in its simplicity; however, it can also present challenges in its lack of control of polymer volume fraction. By contrast, a technique known as solvent annealing has many more parameters which can be difficult to control, but can also be useful in more fine-tuned control of important pattern characteristics.[7–9] In solvent annealing, an environment of solvent vapors is created for absorption into the BCP film. Absorbed solvents can then lower $\chi$ through solvent shielding enough to allow polymers to diffuse and arrange into the self-assembled structures. Additionally, absorption of solvents into each block is generally not equal, resulting in different degrees of swelling in each block. Control over this swelling is possible by carefully choosing solvent vapors with the proper selectivity to each block and controlling the vapor pressures of such solvents.[7–10] While controlling such complex solvent annealing environments is not as simple as thermal annealing, the added control over block volume fraction can be advantageous for precisely tuning self-assembled patterns.

For lithography applications, in-plane vs. out-of-plane orientation of BCP domains is another critical parameter for the final pattern morphology. For example, in-plane cylinders are useful as line patterns, where as out-of plane cylinders are useful for circle or hole structures. Domain orientation is dominated by the difference in surface energy between the two blocks. Therefore, it can be difficult to achieve lamellae or cylinders perpendicular to the substrate without the use of

blocks with similar surface energy or neutralizing brushes and top-coats.[11–14] For the polymer used in this work, polystyrene-block-polydimethylsiloxane (PS-b-PDMS), the difference in surface energy between PS and PDMS causes a layer of PDMS to form at the air interface, making out-of-plane structures difficult to achieve except in thicker films.[15] This work therefore focuses on creation of line and circle structures by in-plane cylinders and spheres, which more easily form under the layer of PDMS. The removal of this layer is explained in the pattern development section of the methods chapter.

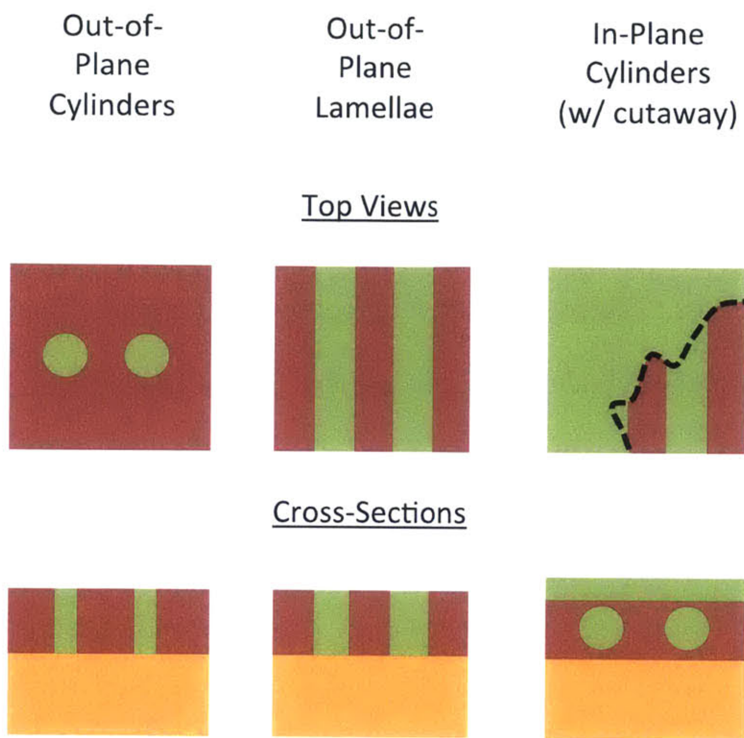


**Figure 1.3** Examples of in-plane and out-of-plane morphologies. The in-plane cylinders are illustrated in the case where the minority block preferentially wets the surface, so a cutaway is shown for the top view.

BCPs can readily form ordered periodic patterns of these described morphologies over short ranges; however, large area patterns generally lack long range order.[16,17] With the addition of a template patterns, BCPs have been shown form low-defect, highly ordered patterns over large areas.[16–19] This impartation of long-range order has been shown through many types of template patterns including chemical

templates[11,20,21], trenches[18,22–24], wrinkles[19], and electron-beam-fabricated topographical features[16,17,25–27].

## 1.2 Electron-Beam Lithography for BCP Templating

This work focuses on templates for BCPs fabricated by electron-beam (e-beam) lithography (EBL). EBL is a widely utilized nanofabrication technique capable of sub-10 nm features.[28–32] By exposing a resist to high-energy electrons in a focused beam, the resist can be altered and made soluble or insoluble to a developer depending on whether the resists operates as a positive tone or negative tone resist. As illustrated by the process in Figure 1.4, a positive-tone resist becomes soluble only in the exposed region, while a negative-tone resist is soluble in its developer everywhere but the exposed region.

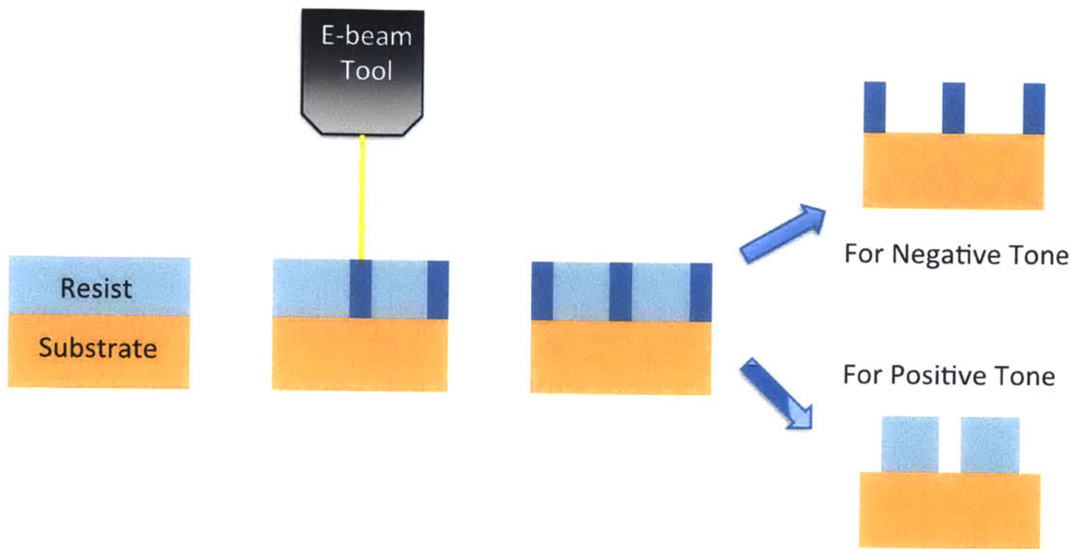


**Figure 1.4** Cartoon of illustration of the e-beam fabrication process and positive vs negative tone resist. After HSQ deposition, patterns are exposed via EBL. The resulting pattern is then developed, where the exposed regions is removed if the resist was positive tone, or the unexposed region is removed if the resist was negative tone.

A common negative-tone resist for use in EBL is hydrogen silsesquioxane (HSQ).[28–32] Figure 1.5 shows an example of a fairly high-resolution structure of exposed and developed HSQ. HSQ patterns can be developed by a simple 4 minute salty developer process[30], and are also capable of undergoing oxygen plasma ashing after development with minimal etching[26,33], as opposed to polymethyl methacrylate (PMMA), another resist compatible with EBL[27,34,35]. Oxygen plasma ashing can therefore be used with HSQ templates to make the

surface more reactive for chemical functionalization. Functionalizing template surfaces to be compatible with either a BCP's majority[26,33] or minority block[16,17,25] is particularly useful when developing template patterns for BCPs. In this work, HSQ was chosen for its high resolution and material compatibility. Creating a template surface highly incompatible with the minority block is shown to be of critical importance to enabling the most successful results in this thesis. Additionally, the final patterns were then composed of silica like materials resulting from the developed BCP and HSQ.[9,15,36]

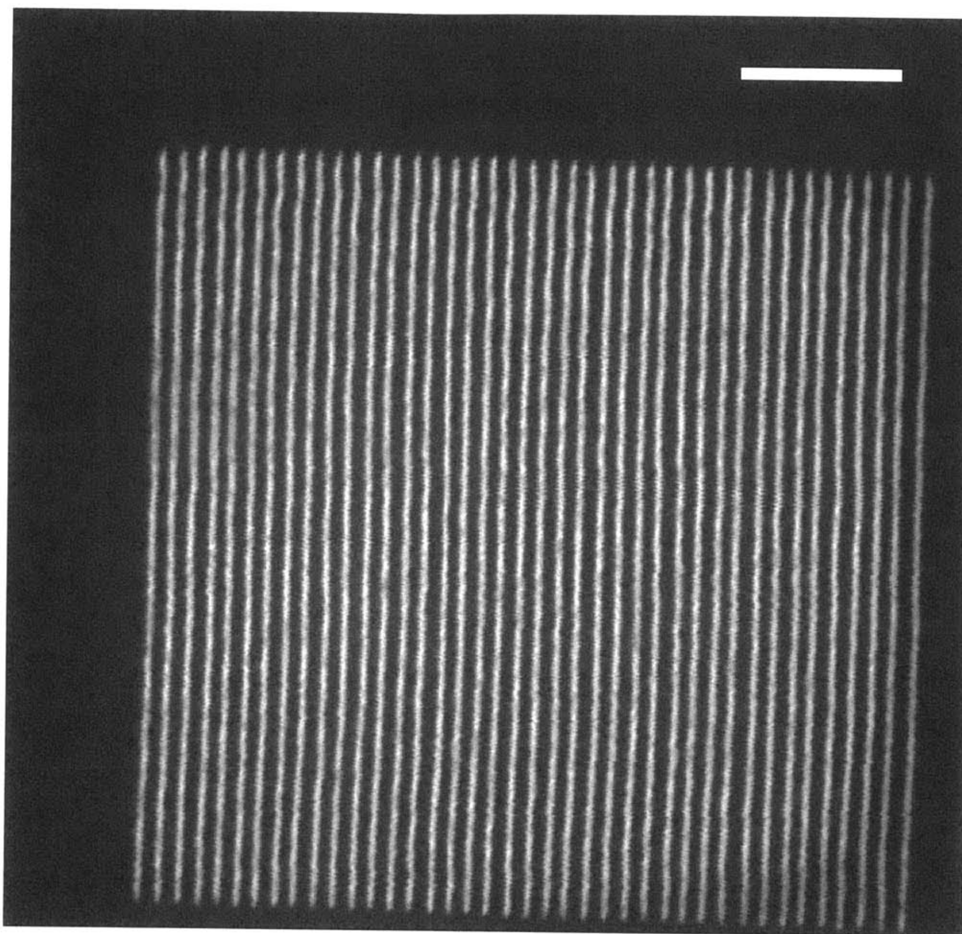

**Figure 1.5** An example of a fairly high-resolution pattern fabricated by EBL and HSQ. The line pattern is 25 nm pitch, and was writtien via line exposures in a 22 nm film of HSQ. Many sturcutres of higher resolution have been fabricated in literature[28–32]. Scale bar is 200 nm.

Templates fabricated by EBL have been utilized to direct the self-assembly of BCPs in many creative strategies. Examples include maintaining ordered BCP patterns over large areas[16,17], altering local BCP morphology[33], orienting and

bending line patterns[17,25], and creating patterns with a removable template after BCP self-assembly[27]. Such strategies, which deeply integrate the e-beam-fabricated template pattern into the BCP matrix, illustrate the high degree of compatibility between EBL and BCP self-assembly, as well as the enhanced patterns possible through combination of these techniques.

## 1.3 Frequency Doubling and Thesis Outline

While typical line doubling techniques generally use complicated deposition and etch-back steps[37,38], this thesis instead explores line doubling by combining the technologies discussed in this introduction chapter. BCP templating by EBL is investigated for its potential to increase pattern density beyond what BCP self-assembly achieves alone. Most successfully, it is shown that the density of BCP line patterns can be doubled by the incorporation of HSQ lines between the in-plane cylindrical microdomains.

The work in this thesis is presented as follows. In Chapter 2, the general process flow, methods, and tools utilized to investigate and develop density doubling are presented. Chapter 3 then presents an investigation of line doubling with high-molecular weight, cylinder-forming PS-b-PDMS. Investigated annealing methods are presented, followed by careful design and surface functionalization of HSQ templates. This investigation led to the successful result of line doubling. Lastly, Chapter 4 provides a few summarizing remarks on the investigations and lessons learned in this thesis.

# Chapter 2

# Methods

This chapter describes the generalized process flows, experimental methods, and tools relevant to the investigated work of density doubling.

## 2.1 Introduction

Directing self-assembly with template patterns was a many step process for each experiment. As such, each step in the overarching experimental process flow required careful investigation and optimization. Figure 2.1 illustrates the general process flow, described briefly in this section with detailed descriptions of the individual steps and tools composing the sections of this chapter.

Experiments investigating directed BCP self-assembly began with e-beam-fabricated arrays of varried template patterns upon a silicon substrate, while experiments investigating BCP self-assembly alone began with only a blank silicon substrate. Additionally some experiments isolated template exposure or development parameters, in which case, fabricated templates proceeded with no further processing outside of image analysis. After functionalizing either just the

bare silicon substrate or the silicon and template pattern, the appropriate BCP was deposited, and the sample placed within an annealing apparatus. Samples were subsequently developed, leaving the minority block of the self-assembled pattern and any existing template pattern. The patterns were then observed under a scanning electron microscope (SEM) for analysis and adjustment to the investigated parameter.

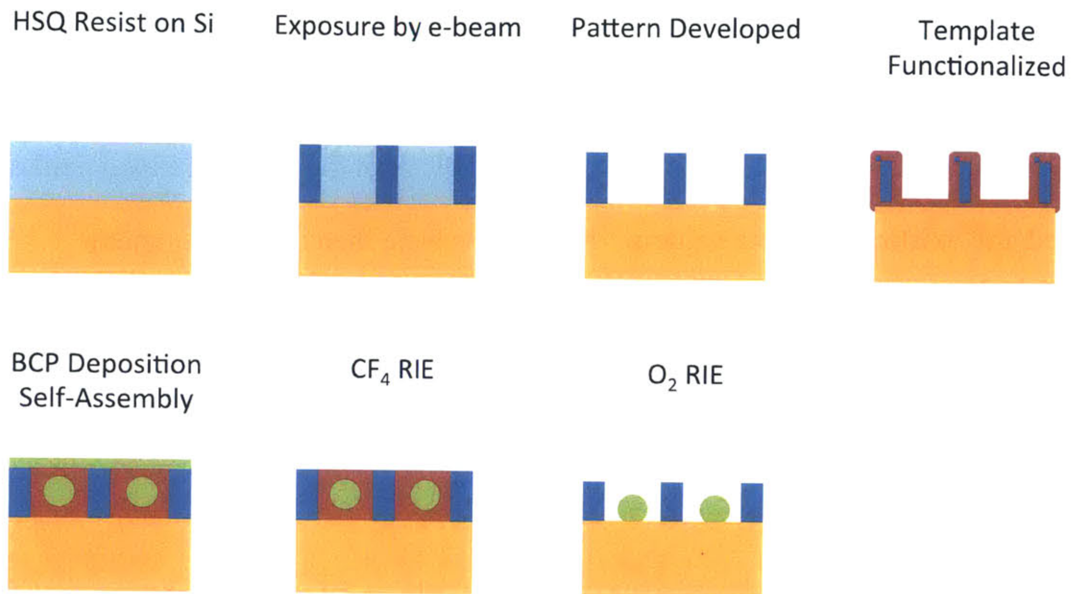


**Figure 2.1** General process flow from left-to-right and down. HSQ resist is deposited followed by e-beam exposure. The unexposed regions are removed by developer. The fabricated template patterns undergoe functionalization to make them selective the the BCP majority block. The prepared template pattern is then used to directed self-assembly within the template region. Post-anneal, the PDMS layer is removed by $CF_4$ RIE, and the PS-matrix (and brush) are removed by $O_2$ RIE

## 2.2 E-Beam Template Patterns

In the case of experiments investigating either template fabrication or directed self-assembly, the first processing steps fabricated template patterns upon blank

silicon substrates. HSQ was first deposited on silicon by spin coating a solution of 2% HSQ dissolved in methyl isobutyl ketone (MIBK) at several spin speeds. After a 15 min warm-up procedure to stabilize its light source, a Filmetrics F20 reflectometer was used to measure HSQ thickness and select the sample with desired film thickness, or if necessary, adjust the range of spin speeds for achieving target thickness. Appropriate spin speeds for a given HSQ film thicknesses varried based on the age and quality of the HSQ, as well as environmental conditions which have yet to be isolated. HSQ films in the range of roughly 20 - 40 nm were utilized depending on the desired line height for a given experiment.

After preparation of HSQ films upon silicon, patterns were written via EBL. Patterns were exposed with a Raith 150 scanning electron-beam lithography system, operating at 30 keV with a 30 μm objective aperture and 6 mm working distance. Lines were fabricated either by line exposure or rectangular area exposure. Arrays of template patterns were fabricated on each sample with varried dose, feature frequency, and rectangle width if area exposure features were used. Dose variation was necessary for initial calibration to HSQ film thickness, varying line width, and compensating local feature dose for proximity effect[32,39]. Feature frequency variation was necessary for observing BCP self-assembly response at differing degrees of constraint or commensuration with $L_0$.

Exposed patterns were developed using a salty developer method. Samples were immersed in the salty developer solution, deionized water with 4% NaCl and 1% NaOH by weight, at approximately 24°C for 4 minutes, and then rinsed for 2 min under a stream of deionized water before being rapidly dried by compressed $N_2$ gas[30].

## 2.3 Surface Functionalization

Substrates were functionalized with a polymer brush matching the chemistry of the majority block, in this case, PS. Majority-block-functionalization was necessary for creating a pattern where PDMS cylinders assembled between template lines instead of adhering to them. Experiments targeted at BCP self-assembly alone, which did not require a prepared template, still utilized PS-functionalization on the blank silicon substrate to maintain consistent surface chemistry between templated and non-templated experiments. Experiments which investigated self-assemlby with templating began with HSQ templates upon silicon. To maximize brush adherence to template sidewalls, an oxygen plasma ashing step was also performed on template-containing substrates. Ashing was performed under a plasma of 80% He and 20% $O_2$ at 0.35 Torr and 50 W for 2 min. This exposure maximized the available bonding sites for the hydroxyl-terminated PS brush and transformed[15] the HSQ pattern into a silica-like material.

Functionalization of either such template-containing substrates or blank silicon substrates were then carried out by the following steps. A solution of 1%, by

weight, hydroxyl-terminate PS brush dissolved in toluene was spin-coated upon substrates at a speed of 5000rpm and minimum acceleration provided by the spin coater. The substrates were then placed under a 20 Torr vacuum and heated to 170°C. After 14 to 18 hours, substrates were removed and PS brush molecules that had not bonded to the substrate or template surfaces was removed by a 15 min immersion in toluene and 15 s toluene rinse. The most common molecular weight of PS brush used was 1.2 kg $mol^{-1}$; however, larger brush polymers were also investigated, as described in Chapter 3, with molecular weights up to 28 kg $mol^{-1}$.

## 2.4 BCP Deposition

BCP films were deposited by combined spin coating and reflectometer measurement. Solutions consisted of BCPs dissolved in rapidly evaporating solvents. The rapid evaporation of solvents during pipetting and spinner acceleration made spin coating sensitive to atmospheric conditions and speed of solution deposition. To achieve the target thicknesses within 5 nm, as was often required to achieve exactly one full layer of microdomains, a Filmetrics F20 reflectometer was employed for measuring the film thickness. Measurements were made after a 15 min warm-up procedure, to stabilize the light source.

PS-b-PDMS BCPs were utilized for their high etch selectivity[15,24] by reactive ion etching (RIE) with PDMS conversion into silica-like material[9,36], high $\chi$ value[15,40], and previous group experience annealing polymers of this material make-up.

## 2.5 Annealing Apparatuses

BCP self-assembly was explored by many annealing methods carried out in four different annealing apparatuses. These setups are described here. While the first apparatus was a simple vacuum oven for thermal annealing, more complex setups were utilized for solvent annealing. Figure 2.2 provides a cartoon illustration of these setups in addition to their descriptions below.

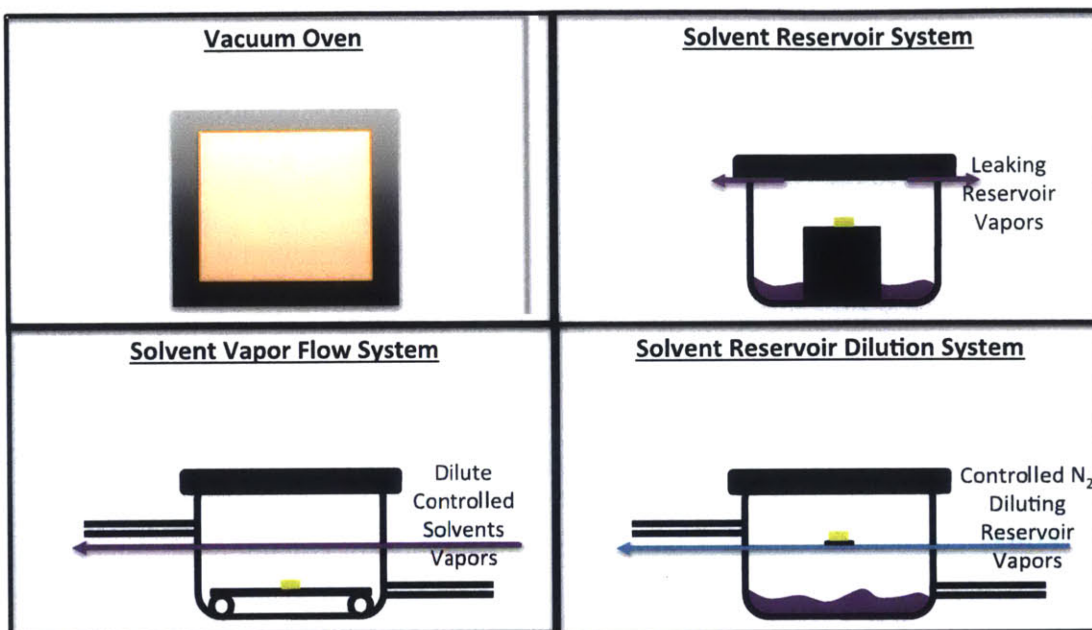


**Figure 2.2** Annealing Apparatuses cartoons. The vacuum oven was used for thermal annealing. The solvent reservoir system utilized a chamber leak to slightly dilute solvent vapors from the reservoir. The solvent vapor flow system controllably introduced solvent vapors to the chamber by mass-flow-controlled bubling of externally connected solvents, and further diluting these solvents with mass-flow-controlled $N_2$ gas. The solvent reservoir dilution system introduces solvent vapors by a reservoir and controlles dilution of vapors by connected, mass-flow-controlled, $N_2$ gas.

The apparatus referred to as the solvent reservoir system consisted of a sample stage and solvent pool within an imperfectly sealed chamber.[8,27] The imperfect seal allowed for a controlled leak of solvent vapors from the solvent pool beneath

and around the sample stage. The leak was designed to prevent vapors from reaching high pressures, which could dewet the BCP films. Although some variation in vapor pressures can achieved in such systems by varying the ratio solvent pool surface area to empty chamber space[8], most easily by changing the volume of solvent in the pool, this system was most commonly used as a simple setup for high vapor pressure annealing experiments which did not require significant variation in vapor pressure. Solvents could be easily changed by cleaning the chamber and depositing different solvents or solvent mixtures into the reservoir; however, some solvents with high vapor pressures proved difficult for the system.

The solvent vapor flow system, as it is referred to here, consisted of a sample stage within a chamber connected to a controlled flow of solvent vapors[10]. Vapors were introduced through mass-flow-controlled bubbling of solvent vapors by $N_2$ gas. Separate chambers housed different solvents connected to lines for the generated solvent vapors to be pushed down. Bubbling rates from each chamber could be controlled individually before vapor lines were mixed and optionally diluted further by an additional line of $N_2$ gas. Mixing of solvents could also be accomplished in liquid form before bubbling. Final mixed and diluted vapors flowed through the annealing chamber connected down stream. This system was useful for experiments focused on varying vapor pressures, but changing solvents

required cleaning and purging many of the components in an annealing channel, making the system less ideal for experiments involving many different solvents.

A third system, developed by fellow students, was used in some of the latter stages of this work. Referred to in this work as the solvent reservoir dilution system, this setup consisted of a small sample stage above a solvent pool, within a chamber connected to a mass-flow-controlled line of $N_2$ gas. This system provided great flexibility for investigating various annealing solvents at varried vapor pressures. Solvents could be quickly changed by cleaning the annealing chamber, and depositing new solvents or solvent mixtures into the solvent pool, since the line feeding into the chamber was only $N_2$ gas. Varried $N_2$ flow rates were used to dilute the vapors evaporating from the solvent pool below the sample.

## 2.6 Pattern Development

After annealing the deposited BCP films, the self-assembled patterns were developed by RIE[9]. Due to surface energy difference between PS and PDMS, the self-assembled patterns in PS-b-PDMS formed a layer of PDMS at the air interface[9,16,24,36]. A 5 s RIE of $CF_4$ at 50 W and 15 mTorr was first used to remove this top layer. The matrix of PS was then selectively removed via 22s RIE of $O_2$ at 90 W and 6 mTorr. This latter step also oxidized the PDMS domains leaving behind a silica-like nanopattern[9,36], which could be analyzed under SEM.

## 2.7 Metrology

Several SEM tools were utilized for pattern imaging. Top down images were captured on a Raith 150 scanning electron beam lithography tool operated 10 keV. Tilted images were acquired via Zeiss Merlin SEM operated at 8 keV or Helios Nanolab 600 Dual Beam tool operated at 10 keV. The captured images were the most common form of results. Images were analyzed and used to inform alterations to the process flow; for example, altered BCP annealing conditions or changes to template fabrication.

# Chapter 3

# Line Doubling via Directed Self-Assembly of High Molecular Weight, Cylinder-Forming BCP

This chapter describes the templating and self-assembly of high molecular weight, cylinder-forming BCP for the creation of high-density patterns. This chapter describes the design and fabrication of template patterns, as well as the combination of these templates with optimized self-assembly annealing methods. The resulting line patterns were optimized to achieve a combined template-BCP frequency double that which was achieved in the BCP alone.

## 3.1 Introduction

One of the major uses for BCP self-assembly is as method for enhancing density of patterns in combination with other fabrication processes.[41,42] Attempting to enhance the resolution of BCP patterns is therefore of great importance for fabrication devices with increasingly dense features. Utilizing BCPs with decreasing molecular weights is one method to fabricate smaller features as $L_0$, the

period between BCP microdomains, is reduced with decreasing degree of polymerization, $N$.[1,2] However, polymers with increasing $\chi$ must be developed to maintain $\chi N$ at large enough values for self-assembly.[1,2] As maintaining this strong segregation becomes increasingly difficult for low molecular weight BCPs, methods capable of enhancing BCP pattern density can prove useful.

Several approaches have been investigated for BCP line doubling thus far. Similar to traditional methods of line doubling[37,38], BCPs have been doubled through steps of spacer deposition and etch back[43]. BCP line doubling, without these complicated deposition and etch back steps has also been demonstrated, through self-assembly of bilayer cylinders.[36,44] Through self-assembly optimization and etch contrast, the bilayer cylinders with diameters well under 50% of $L_0$ were achieved, preventing overlap of lines from the top and bottom layers on removal of the majority block. The work presented in this chapter utilizes a majority-block-functionalized, e-beam-fabricated template for BCP line doubling. The pattern of lines is both deeply integrated into the BCP matrix and of matching periodicity to the BCP, thereby doubling line density over the BCP alone.

Although the final pattern appears as template lines inserted to double the BCP lines, the actual process order, as explained in Chapter 2, first fabricates and functionalizes the template, and then allows BCP to infiltrate and self-assemble within the template. In this approach pitches could be varried and were not required to match the BCP's pitch, $L_0$, exactly. Even successful application of

template pitches below $2L_0$ achieves an increase in pattern density, it is only when requiring a density increase corresponding to doubling or better that a template pitch of $L_0$ or less is required. However, as template patterns approached $L_0$, the goal of a 50% duty cycle, or equal line and gap width, was challenged as indicated in Figure 3.1. In an attempt to address this issue of duty cycle, and observed PDMS-HSQ collision defects, several additional annealing methods were investigated in an attempt to increase the swelling ratio of PS to PDMS. Also, as detailed in the template design section, multiple brush lengths were also investigated to address these issues.

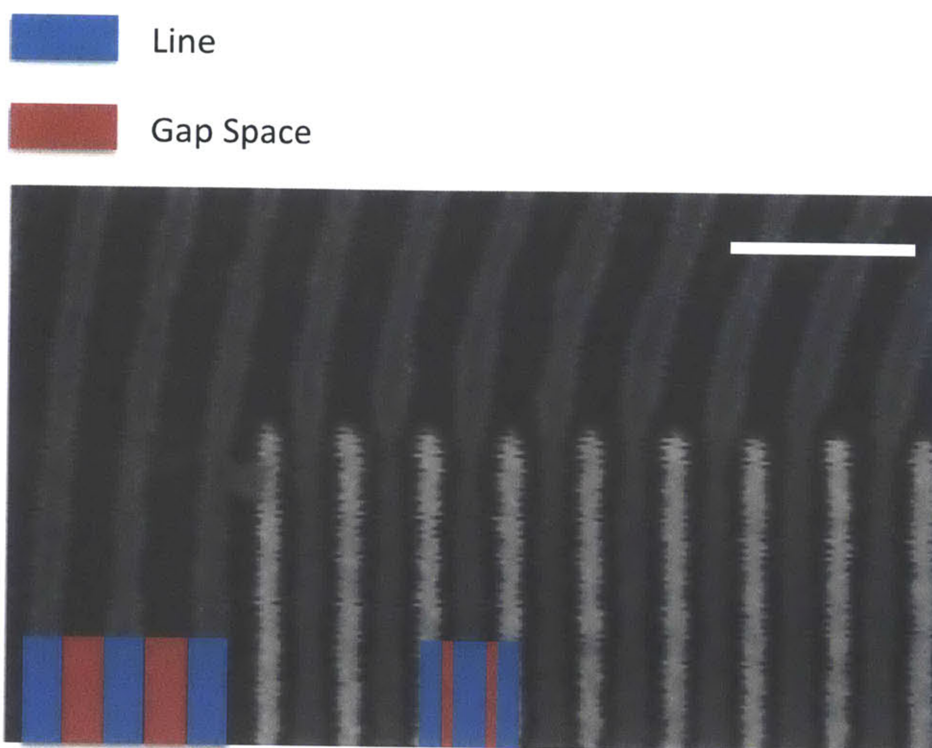


**Figure 3.1** Poor duty cylcle within narrow template patterns. The template pitch here is 45 nm, nearly $L_0$ (44 nm). As illustrated by the graphic overlays, the gap space between lines is similar to line width for patterns outside the template, while inside the template, gap space is very narrow in comparison to line width. The scale bar in the upper right corner is 100 nm.

## 3.2 Annealing Methods

Investigation of annealing methods was a significant portion of this work. The majority of annealing methods which were explored utilized cylinder-forming 45.5 kg mol$^{-1}$ PS-b-PDMS. This polymer consisted of a 31.0 kg mol$^{-1}$ PS block

and a 14.5 kg $mol^{-1}$ PDMS block. The volume fraction of PDMS was 32%, leading to cylindrical morphologies during anneals that did not largely alter this volume fraction. Sphere-forming PS-b-PDMS was also utilized during anneals designed to swell the polymer from a spherical to cylindrical phase.

### 3.2.1 Thermal Annealing

Thermal annealing was investigated for the simplicity offered by only optimizing two parameters, temperature and time. Unfortunately, thermal annealing was unable to provide sufficient mobility to the utilized 45.5 kg $mol^{-1}$ PS-b-PDMS polymer, resulting in only polymer micelles instead of ordered, self-assembled structures. An example of such micelles remaining after 48 hours of thermal annealing at 170° C is shown Figure 3.2.

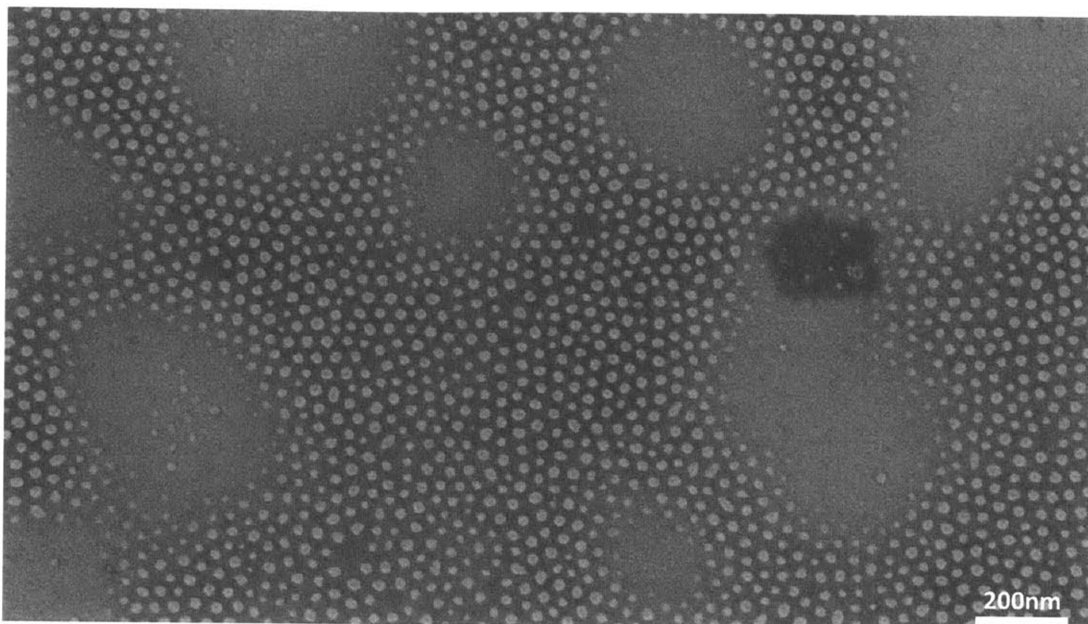


**Figure 3.2** Failed thermal annealing of 45.5 kg $mol^{-1}$ PS-b-PDMS. It was believed the sphereical structures were polymer micelles and not the result of the BCP attempting to assemble into order sphere patterns. Annealing conditions were 170°C for 48hr under vacuum.

### 3.2.2 Controlled Leak of Toluene Vapors

The solvent reservoir system was used with solvents mixtures of toluene and heptane to provide mobility to PS and PDMS blocks, respectively. While varried ratios of toluene and heptane were investigated to achieve the thin PDMS lines, it was eventually found that pure toluene could be used with long anneal times to achieve self-assembly. Toluene provides more selectivity and swelling to PS domains and it is therefore beneficial to maximize the fraction of toluene when

attempting to achieve thin PDMS domains. While heptane is often included in anneals of PS-b-PDMS for imparting mobility or swelling to the PDMS domains, toluene's weak selectivity to PDMS proved high enough to for sufficient mobility and low-defect self-assembly. As shown in Figure 3.3, annealing with pure toluene in this solvent reservoir system achieved ordered, low-defect cylinders, with an average pitch of approximately 44 nm.

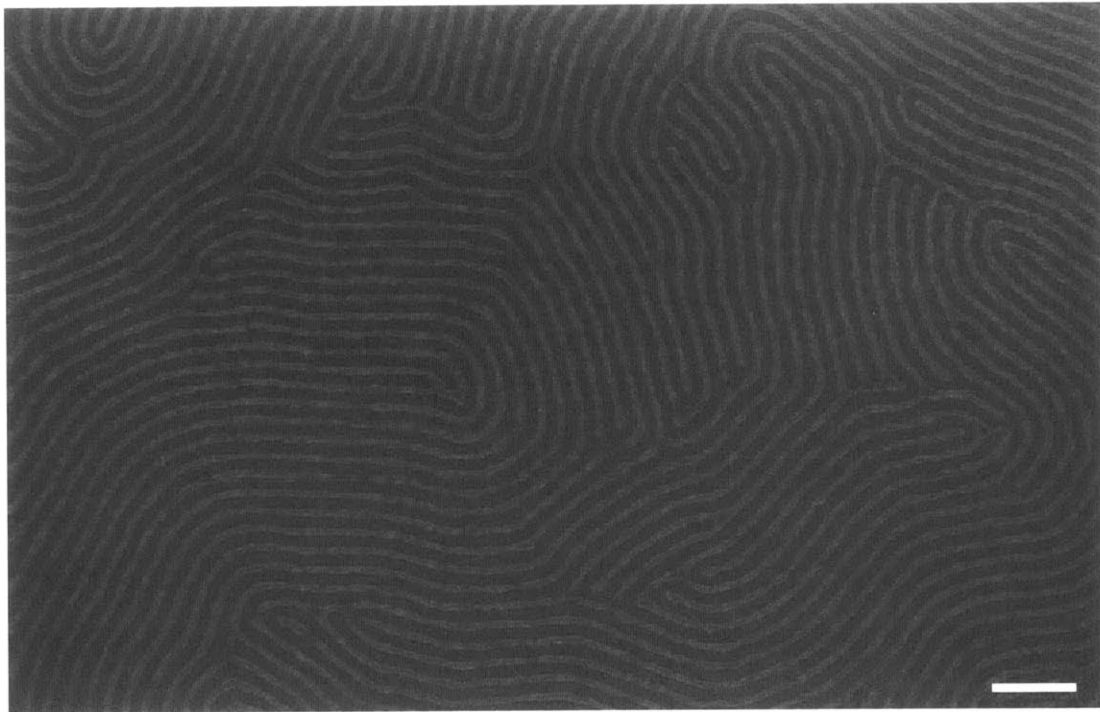

**Figure 3.3** Typical annealing of well ordered cylinders from annealing with toluene in the solvent reservoir system. Although thinner cylinders were desireable for imrpoved duty cycle and defect density. This sample was annealed for 3 hours. The scale bar is 200 nm.

### 3.2.3 Targeted Swelling of PS Domains

A significant difficulty in experiments with line doubling was decreased gap space, composed of PS, between PDMS domains and HSQ lines as template line pitched was decreased towards $L_0$, where line doubling was to occur. Beyond the ideal goal of a 50% duty cycle after line doubling, it was also desired to increase this PS-gap as a possible method for preventing PDMS-HSQ collision defects also observed as pitches were lowered. One approach taken was to attempt to optimize annealing conditions that would increase the swelling ratio of PS to PDMS over what was achieved in pure toluene anneals.

For flexibility with annealing solvents and vapor pressures, experiments were carried out in the solvent reservoir dilution system. Solvents of chloroform and acetone were investigated based on their selectivity. Chloroform had a solubility parameter of 18.7 $(MPa)^{1/2}$, and acetone had a solubility parameter of 19.7 $(MPa)^{1/2}$.[18,45] By comparison, toluene's solubility parameter of 18.3 $(MPa)^{1/2}$ was successful in annealing the utilized PS-b-PDMS, with PS having a solubility parameter of 18.5 $(MPa)^{1/2}$, and PDMS having a solubility parameter of 15.5 $(MPa)^{1/2}$.[18,45] The proximity of chloroform and PS solubility parameters was similar to that of toluene and PS, while the chloroform's solubility parameter was much more distant from the PDMS solubility parameter than toluene was. Acetone though, had a solubility more dissimilar to both PS and PDMS than toluene did, but acetone's solubility parameter was still much nearer in proximity to PS than

PDMS. These solubility parameter values suggested to us that chloroform may have been capable of swelling PS similarly to toluene, but swell PDMS less than toluene; while we believed acetone may have been an alternative solution with possibly even less swelling to the PDMS domain.

A variety of annealing conditions were attempted using these solvents, with the general trend of evolution from either a spherical or micelle structures to thick cylinders with increasing vapor pressure and time. A few examples of these results are pictured in Figure 3.4. While several possibilities exist for the lack of thin cylinders forming under the conditions attempted, we believe the low selectivity to the PDMS domain may inhibit mobility of the BCPs, possibly preventing good microphase separation. While further work may be possible to achieve more promising results, templating methods, explained in subsequent sections, were already capable of promising results with the toluene annealing method.

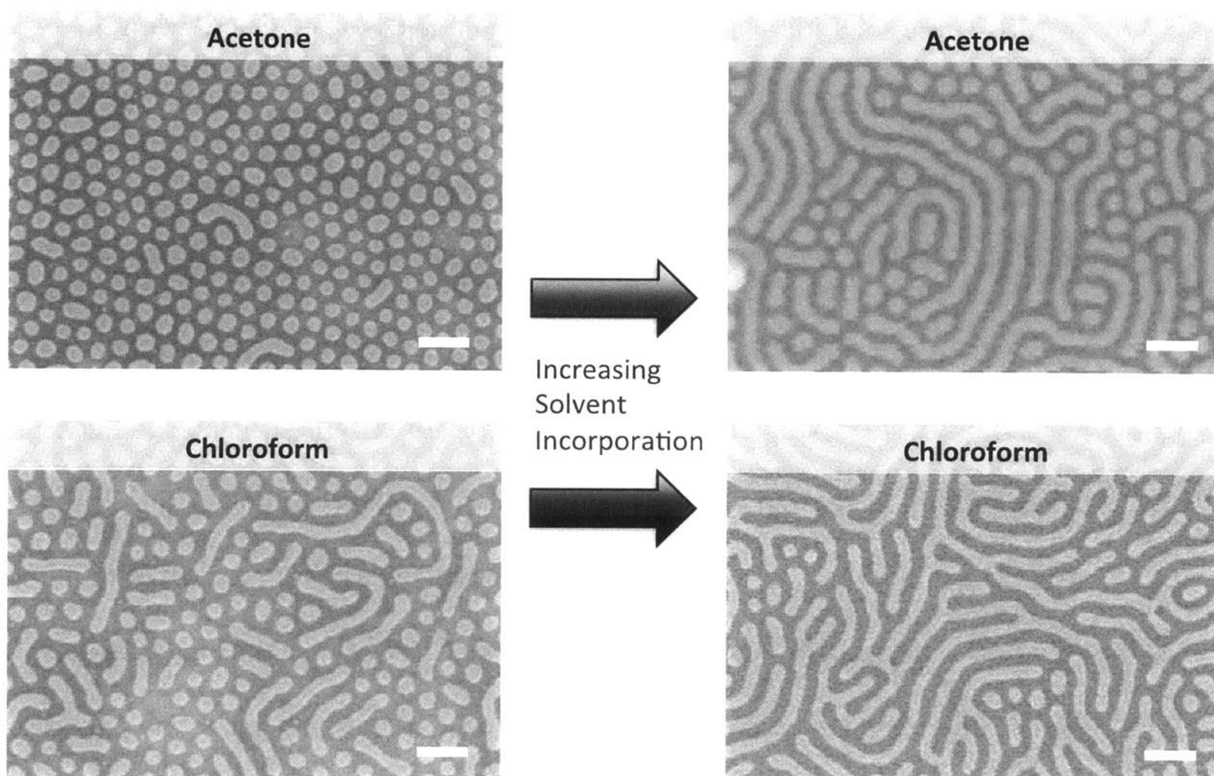


**Figure 3.4** Sample of images showing general evolution arrows for choloroform and acetone. Evolution was from a cylindrical morphology to a thick cylinder morphology with poor order. Scale bars are 100 nm.

### 3.2.4 Cylinders From Sphere-Forming BCP

A different annealing method approach was also attempted for increasing the PS-gap. Instead of attempting to swell cylinder PS domains more or PDMS domains less, as in the previous section, it was attempted to swell the PDMS domain of a spherical morphology. By starting a sphere-forming BCP, i.e. a BCP with much larger PS block than PDMS block, it was attempted to increase the

volume fraction of PDMS during annealing to push the morphology just into the cylinder phase, where cylinders may be closer to their minimum possible size.

In Figure 3.5, a 51.5 kg $mol^{-1}$ PS-b-PDMS BCP (PS=43 kg $mol^{-1}$, PDMS=8.5 kg $mol^{-1}$) is pictured at several different swellings of the PDMS domain. The BCP's typical sphere-forming morphology is shown in Figure 3.4a, annealed within the solvent vapor flow system with 10 sccm bubbling of a cosolvent of 5-to-1 toluene to heptane. In order to swell the PDMS domain in this morphology, some simple anneals were first attempted in the solvent reservoir system using solvent mixtures of toluene and heptane with increased fractions of heptane, the solvent more selective to PDMS.[8,45] Figure 3.4b and Figure 3.4c demonstrate resulting morphologies with increased swelling in the PDMS domain. However, both morphologies were the result of attempted similar annealing conditions. These anneals were 1hr in length with 1 mL of a 1-to-3 mixture of toluene and heptane in the solvent reservoir system. Each sample had significant variation across its surface in the local fraction of cylinder or spheres. This variation combined in environmental conditions, which were not isolated, was likely responsible for the observation of differing morphologies while under attempted similar annealing conditions. Due to these local variations within the film and variations from experiment to experiment, continued annealing investigation was moved to the more isolated conditions of the solvent reservoir dilution system.

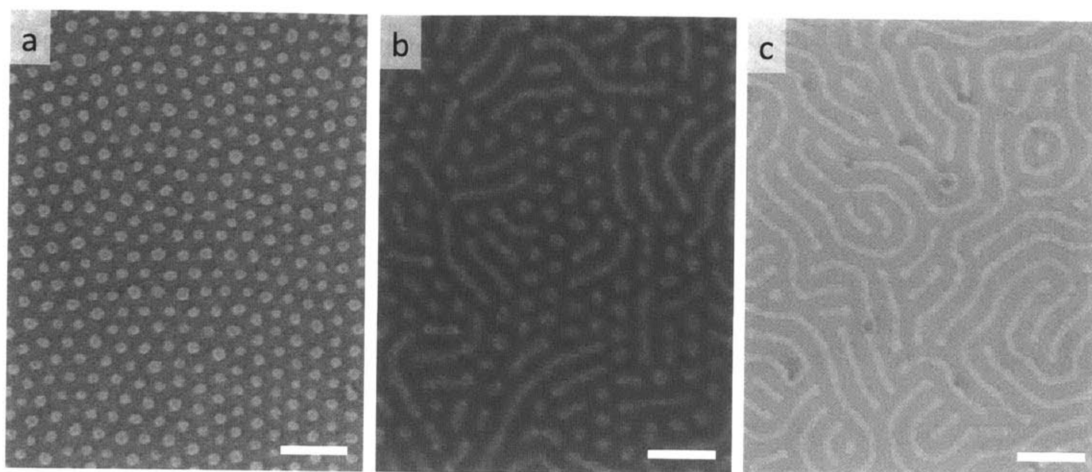


**Figure 3.5** Different degrees of swelling of SD52. a) PDMS domains are not largely swollen. Since the BCP begins with a very large PS block, spherical morphology is present. b) increased swelling of the PDMS domains moved the film to the borderline of spherical and cylindrical phases. c) Most spheres are swollen to cylinders. Scale bars are 100nm.

Using a 4 mL solvent mixture of 1-to-3 toluene to heptane with the solvent reservoir dilution system, swelling of PDMS domains was investigated under varried vapor pressures and anneal times. A sphere-forming 56.1 kg $mol^{-1}$ PS-b-PDMS BCP (PS=47.1 kg $mol^{-1}$, PDMS=9.0 kg $mol^{-1}$) was utilized due to material availability. Although some initial increase was observed in sphere and cylinder connectivity for increased vapor pressures or anneal times, self-assembly generally appeared to settle to a morphology of short, poorly-ordered cylinders. Figure 3.6 shows a sample of the anneals, where vapor pressure was at a constant

dilution of 1 sccm $N_2$ for several anneal times from 10 min to 120 min. The images illustrate how some of the initial increase in cylinder connectivity is observable in the 10 min to 30 min images, while little or no increase is observable in connectivity or order as annealing time is increased further.

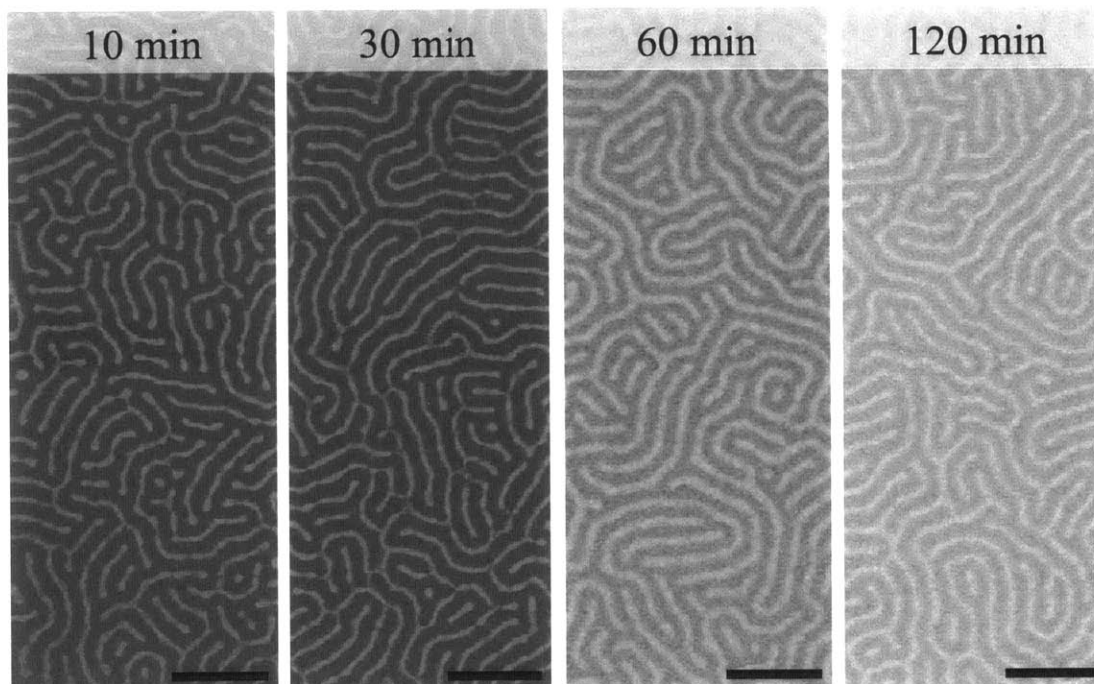


**Figure 3.6** Sampling of anneal times for 56 kg $mol^{-1}$ PS-b-PDMS annealed in the solvent reservoir dilution system under a mixture of 1-to-3 toluene to heptane, diluted by 1 sccm of $N_2$ gas. Although some minor changes in cylinder connectivity and possibly order were observed early on, continued annealing provided little or no improvement in ordering, indicating low mobility for BCPs in these anneals. Scale Bars are 200nm.

The observed lack of, or extremely slow, increase in order was a major drawback to this method, as good order and mobility were desirable for BCPs to infiltrate template patterns. Therefore, the toluene annealing method was ultimately selected for templating experiments in place of this PDMS-swelling method.

## 3.3 Directed Self-Assembly

In this section, directed self-assembly is discussed using the selected annealing method of the solvent reservoir system with toluene. The design of geometric template parameters is first described followed by the investigation of varried brush length. This latter investigation addresses the defectivity issues encountered in narrow template patterns and ultimately achieves line doubling; however, the final pattern's duty cycle was still problematic.

### 3.3.1 Template Design

Templates were designed as line patterns selective to the PS domain, causing PDMS cylinders to often self-assemble between the functionalize HSQ lines. To better isolate and understand defects and failures, template patterns were designed to investigate self-assembly under differing degrees of strain. This was approached by preparing samples with a range of template patterns with varried line widths and line spacing, both larger and smaller than the BCP's cylinder spacing and cylinder width, respectively. While setting the pitch of lines was a simple parameter, developed line width not tied to a single input parameter. This variation

was a result of dose varying with pitch due to the proximity effect[32,39], and varried amount of HSQ to be exposed when investigating differing line heights. Therefore, a range of template pitches and doses were fabricated on all samples. Additionally, the area exposure of lines allowed for several base line widths to be input as thin rectangular exposures, and line width further varried from these "base" line widths by changing dose. Some early experiments also used linear exposures for lines and strictly varried line width by dose.

Line height was varried by altering HSQ thickness. In an attempt to maximize the template lines' barrier to collision and overlap with PDMS domains, maximum allowable HSQ thicknesses for the given geometries were pursued. In these closely spaced patterns, capillary collapse[46,47] of lines limited the maximum line height. An example of this collapse is shown in Figure 3.7. Collapse was observed for some narrow and closely spaced lines down through HSQ thicknesses of 36 nm, with little-to-no collapse observed near for HSQ films of 33 nm. These results led to the choice for a nominal HSQ thickness of 31 nm with deviations thickness of ±2 nm still often used for writing.

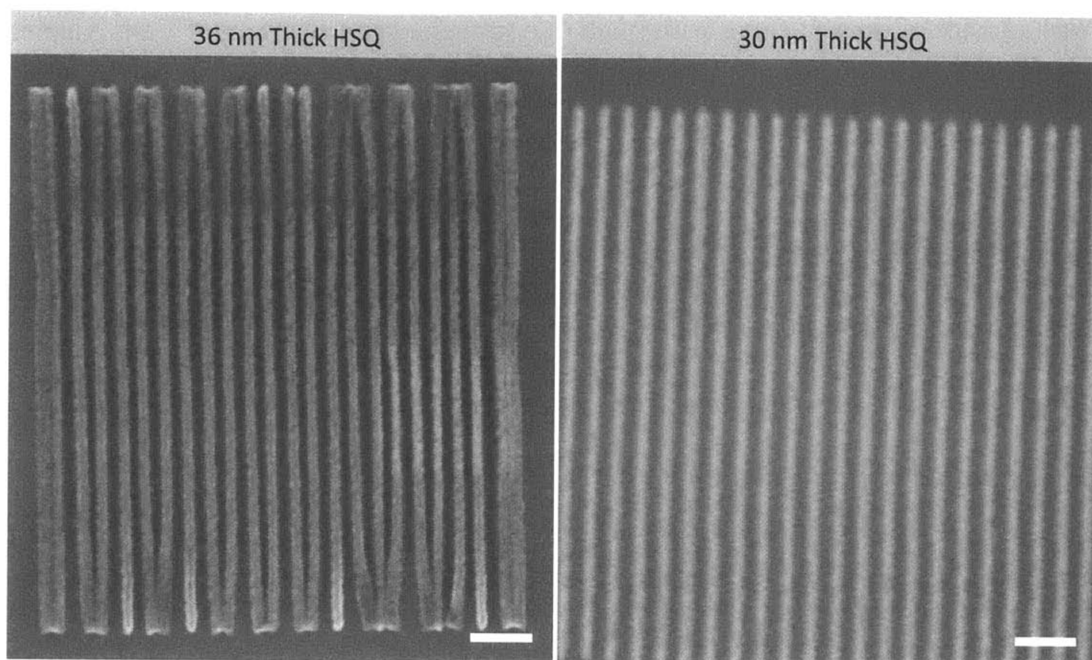


**Figure 3.7** Example of capillary collapse observed for thick HSQ films. The left image shows lines written with a 36 nm thick film of HSQ. The right image shows unollapsed lines due to their lower aspect ratio from writing on a thinner, 30 nm film of HSQ.

Support for the belief that HSQ line height was not too high was provided by the nature of several defect types and similar appearance of line heights under tilt-SEM. As can be seen in Figure 3.8, PDMS cylinder height does not appear greatly diminished next to the HSQ lines, and during solvent annealing, the PDMS cylinders are raised in height due to the surrounding PS matrix and film swelling[7,36]. Additionally, the defects pictured in Figure 3.8 show several cylinders

connected over HSQ lines, which may indicate PDMS cylinders assembled at a height above or near the top of the HSQ lines, before subsequently collapsing during quenching of the anneal and RIE development.

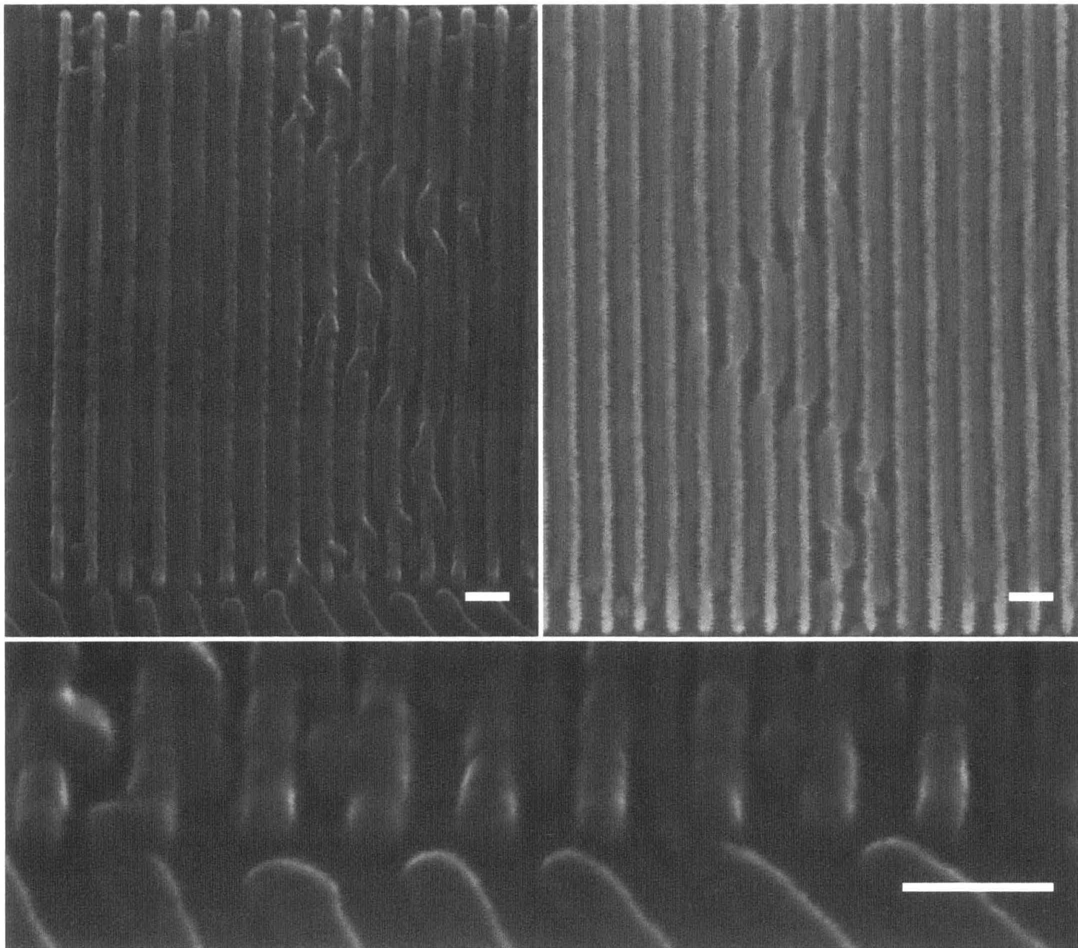

**Figure 3.8** Support for HSQ lines not being too tall. The top images show examples of an intermittently observed defect. While less clear from traditional SEM (top-right), tilt SEM (top-left) more clearly resolves the defects. PDMS domains appear to be collapsing over the HSQ lines indicating the BCP may have been assembling above the HSQ lines. A higher magnification of the same template pattern (bottom) show the PDMS domains in their unswelled, collapesed state maintain slightly shorter, but similar heights to the HSQ lines. HSQ films in these images were spun to 30 nm thick. Scale bars are 50nm.

With line height remaining Template designs were thus optimized to line heights corresponding to 31±2 nm HSQ films. Fabrication patterns remained in use of a range of varried templates with varried doses each write in order to achieve a spectrum of line widths and line pitches for investigation of other process parameters outside template geometry. The optimized parameters for this write design were base line widths in the exposure design of 6 nm, 8 nm, and 12 nm, with corresponding aerial dose ranges of approximately 7300 $\mu C/cm^2$ to 13500 $\mu C/cm^2$, 7900 $\mu C/cm^2$ to 14000 $\mu C/cm^2$, and 9000 $\mu C/cm^2$ to 15100 $\mu C/cm^2$, respectively.

### 3.3.2 Importance of Brush Length

Brush length was a key parameter for enabling low-defect self-assembly in narrow template patterns. As mentioned above, when template pitches were lowered to approach $L_0$, defects began to appear of PDMS domains touching the template lines. An approach discussed in this section was to compare the effect differing brush lengths had on these defects.

Previously, an extremely small PS brush was used of 1.2 kg $mol^{-1}$ was used in an attempt to maximize the grafting of the brush onto surfaces. However, with this brush, defects began to appear for template pitches well above $L_0$. When longer brushes were used, defects densities were reduced and observed at lower pitches.

Figure 3.9 shows a comparison of BCP self-assembly within template patterns around line pitches of $L_0$. The left image was of a template functionalized by 1.2 kg mol$^{-1}$ brush and shows an example of the common defects experienced well above template pitch of $L_0$. The right image was of a template functionalized by 28 kg mol$^{-1}$ brush and shows an example of the often defect-free assembly at $L_0$.

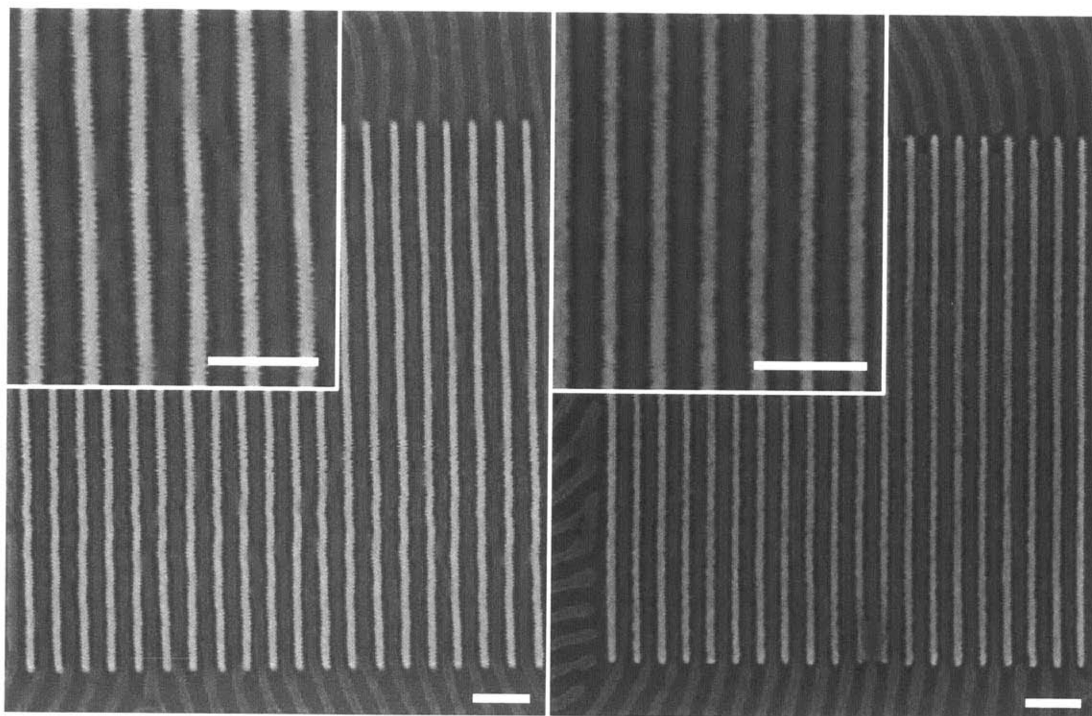

**Figure 3.9** Comparison of typical defectivity in template pitches nearing $L_0$ (44 nm), for small, 1.2 kg mol$^{-1}$, brush (left), and large, 28 kg mol$^{-1}$, brush (right). The left images shows defects occuring in a template of pitch above $L_0$ at 48 nm, while the right images shows an example of low defect self-assembly within a template pitch of $L_0$ (achieving line doubling).

Even with the longest brushes some defects still occurred. These defects became more prevalent with further decrease of template pitch below $L_0$. However, careful inspection of these defects revealed a possible qualitative difference in the type of defect that occurred. Figure 3.10 shows an example comparison of common defects that occurred with high and low molecular weight brushes (again, 28 kg $mol^{-1}$ and 1.2 kg $mol^{-1}$), near and below template pitches of $L_0$. Defects for the small brush appeared to occur in a spatially sharp manner. By comparison, the large brush samples appeared to have PDMS domains, which moved to the HSQ walls in spatially broad manner.

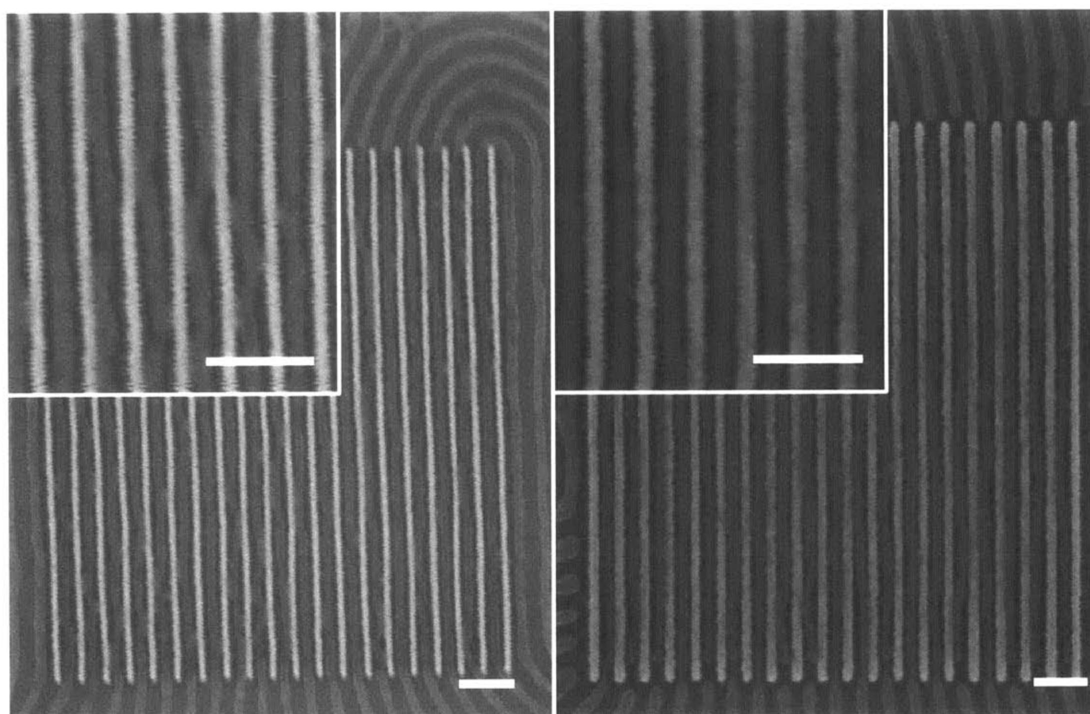

**Figure 3.10** Qualitative comparison of defects observed for small brush (left) and large brush(right).

In order to better observe and understand these defects, tilt SEM was applied for imaging. Two key images are shown in Figure 3.11 below. The left image corresponds to the 28 kg $mol^{-1}$ brush sample while the right image corresponds to the 1.2 kg $mol^{-1}$ brush sample. These images may suggest a qualitative difference the type of defectivity occurring between the small and large brush samples. From the small brush image in Figure 3.11, it appears the PDMS domain may be sticking to the HSQ sidewall, possibly due to the small volume of PS on the HSQ sidewall. In contrast, the PDMS domains within the large brush template pattern appear vertically distorted to an oval-like cross-section. This distortion, in combination with the spatially broad variation of the PDMS domain, may suggest the defect occurs due to collapse of the narrow structure during quenching or RIE pattern development.

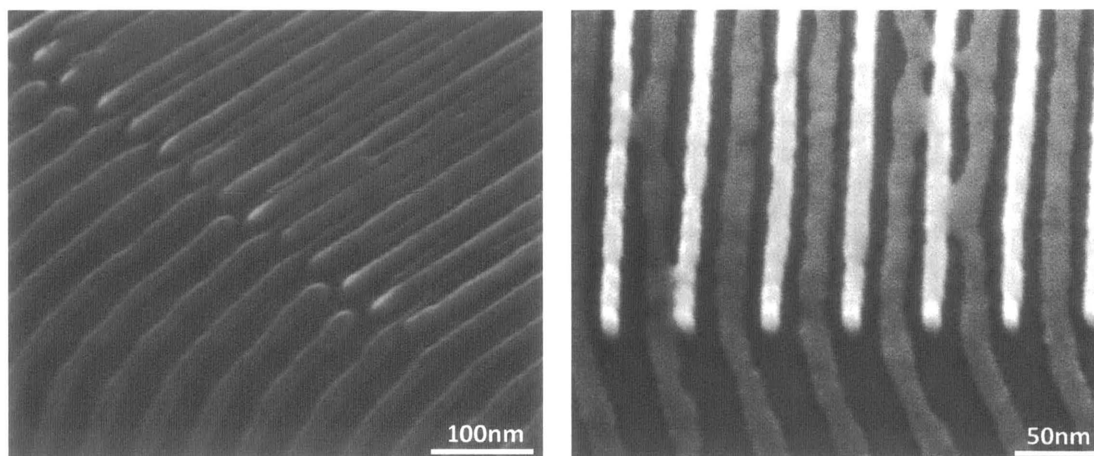


**Figure 3.11** Qualitative comparison of defects observed for small brush (right) and large brush (left). The large brush appears to cause some distortion of the PDMS domain. This distortion and possible subsequent collapse may be responsible for the defects observed with large brushes. This would be in contrast to the qualitative nature of defects observed for the low molecular weight brush.

# Chapter 4

# Summary

This thesis investigated increasing the density of lines from block copolymer patterns by addition of HSQ template patterns. After optimizing several parameters, density increases were great enough to achieve full doubling in density of lines beyond what the BCP was capable of alone.

In Chapter 1, BCPs were introduced along with their mechanisms for self-assembly. Their compatibility with, and ability to enhance, other fabrication methods was discussed. Of particular note was their ability to enhance the resolution and throughput of existing fabrication techniques.[41,42] Electron-beam lithography was also introduced as another nanofabrication method, and noted for its superb compatibility and versatility with BCPs[16,17,25–27]. Upon noting the challenges faced with continued scaling of BCP pattern density, a method was proposed, based on established work for directing BCP self-assembly with e-beam-fabricated template patterns, to double the density of BCP lines by fabricating template lines of equal pitch to the BCP's natural pitch, $L_0$.

With the proposed work and motivation explained, Chapter 2 proceeded by explaining the general process flow and tools utilized to accomplish the work in this thesis. The three annealing apparatuses utilized for controlling BCP self-assembly were explained, along with their general use due to their advantages and disadvantages. Also, PS-b-PDMS was introduced as the BCP of choice for this work.

Chapter 3 then presented some of the challenges with this method of line doubling and several experimental approaches to address them. It was found that self-assembly was successful with template pitches well above $L_0$, but as template lines were brought closer, issues of defects and difficulty maintaining a 50% duty cycle were encountered. With these issues in hand, several annealing methods were presented, several with objectives not just of ordered, low-defect cylinders, but also of achieving a larger aerial width ratio of PS to PDMS. It was thought that a larger PS gap between HSQ lines and PDMS cylinders might help decrease PDMS-HSQ collision defects in addition to improving the duty cycle at low template pitches. Swelling the PS domains of cylinder forming BCP was attempted by annealing with solvents of chloroform and acetone. The resulting morphologies contained mixed spheres and thick cylinders, possibly due to the poor selectivity to the PDMS block. Another approach was to use solvent mixtures to swell the PDMS domain of a normally sphere-forming BCP into thin cylindrical domains. While thin cylinders were formed, they were poorly ordered and short.

Ultimately, annealing with toluene vapors in the solvent reservoir system was selected as the annealing method for use with template investigations. Although this method yielded fairly thick cylinders, the cylinders were well ordered and easily templated.

Defects at low template pitches were ultimately addressed by increased PS brush lengths. PDMS-HSQ collisions prevented low-defect self-assembly within templates, brushed by low molecular weight (1.2 kg $mol^{-1}$) PS brush, as HSQ pitches decreased towards $L_0$. Directed self-assembly was attempted with longer brushes up to 28 kg $mol^{-1}$, which suppressed defects to the point of achieving many low-defect patterns of self-assembled cylinders within template patterns of pitch $L_0$.

Beyond this successful result of line doubling, the self-assembly defects in large-brushed template patterns were investigated. Tilt SEM images revealed a possible qualitative difference between the defects occurring at large pitches in small-brushed templates and defects occurring at small pitches in large-brushed templates. It was suggested that this difference may indicate compressed, laterally narrow PDMS domains which collapse either during RIE development or the quenching step of solvent annealing.

In conclusion, the investigation described in this thesis demonstrated a method for doubling the lines of a BCP pattern by integration of an e-beam-fabricated template pattern into the BCP matrix. The narrow line patterns necessary to double

BCP line density appeared to create a large degree of stress on the BCP system, but the resulting defects were successfully addressed by a functionalizing HSQ lines with a high molecular weight PS brush to repel PDMS cylinders. Future work may address the still small gap between PDMS and HSQ. One possible method could be to utilize RIE processes with mixed gases to thin PDMS cylinders during PS-matrix removal.[36]

# References


1. Bates, F. S. & Fredrickson, G. H. Block copolymer thermodynamics: theory and experiment. *Annu. Rev. Phys. Chem.* **41,** 525–57 (1990).

2. Bates, F. & Fredrickson, G. Block copolymers—designer soft materials. *Phys. Today* 32–38 (2008). at <http://scitation.aip.org/content/aip/magazine/physicstoday/article/52/2/10.1063/1.882522>

3. Nunns, A., Ross, C. a. & Manners, I. Synthesis and Bulk Self-Assembly of ABC Star Terpolymers with a Polyferrocenylsilane Metalloblock. *Macromolecules* **46,** 2628–2635 (2013).

4. Aissou, K., Nunns, A., Manners, I. & Ross, C. a. Square and rectangular symmetry tiles from bulk and thin film 3-miktoarm star terpolymers. *Small* **9,** 4077–84 (2013).

5. Ross, C. a. *et al.* Si-containing block copolymers for self-assembled nanolithography. *J. Vac. Sci. Technol. B Microelectron. Nanom. Struct.* **26,** 2489–2494 (2008).

6. Welander, A. *et al.* Rapid directed assembly of block copolymer films at elevated temperatures. *Macromolecules* **41,** 2759–2761 (2008).

7. Jeong, J. W., Park, W. I., Kim, M. J., Ross, C. A. & Jung, Y. S. Highly Tunable Self-Assembled Nanostructures from a Poly (2-vinylpyridine-b-dimethylsiloxane) Block Copolymer. *Nano Lett.* 4095–4101 (2011). at <http://pubs.acs.org/doi/abs/10.1021/nl2016224>

8. Jung, Y. S. & Ross, C. A. Solvent-Vapor-Induced Tunability of Self-Assembled Block Copolymer Patterns. *Adv. Mater.* **21,** 2540–2545 (2009).

9. Son, J. G., Hannon, A. F., Gotrik, K. W., Alexander-Katz, A. & Ross, C. A. Hierarchical nanostructures by sequential self-assembly of styrene-dimethylsiloxane block copolymers of different periods. *Adv. Mater.* **23,** 634–9 (2011).

10. Gotrik, K. W. *et al.* Morphology control in block copolymer films using mixed solvent vapors. *ACS Nano* **6,** 8052–9 (2012).

11. Liu, G. *et al.* Morphology of Lamellae-Forming Block Copolymer Films between Two Orthogonal Chemically Nanopatterned Striped Surfaces. *Phys. Rev. Lett.* **108,** 065502 (2012).

12. Bates, C., Seshimo, T. & Maher, M. Polarity-Switching Top Coats Enable Orientation of Sub–10-nm Block Copolymer Domains. *Science (80-. ).* 775–779 (2012). at <http://www.sciencemag.org/content/338/6108/775.short>

13. Ji, S. *et al.* Generalization of the Use of Random Copolymers To Control the Wetting Behavior of Block Copolymer Films. *Macromolecules* **41,** 9098–9103 (2008).

14. Huang, E. *et al.* Using Surface Active Random Copolymers To Control the Domain Orientation in Diblock Copolymer Thin Films. *Macromolecules* **31,** 7641–7650 (1998).

15. Son, J. G., Gotrik, K. W. & Ross, C. a. High-Aspect-Ratio Perpendicular Orientation of PS- b -PDMS Thin Films under Solvent Annealing. *ACS Macro Lett.* **1,** 1279–1284 (2012).

16. Bita, I., Yang, J., Jung, Y. & Ross, C. Graphoepitaxy of self-assembled block copolymers on two-dimensional periodic patterned templates. *Science (80-. ).* 939–943 (2008). at <http://www.sciencemag.org/content/321/5891/939.short>

17. Yang, J. K. W. *et al.* Complex self-assembled patterns using sparse commensurate templates with locally varying motifs. *Nat. Nanotechnol.* **5,** 256–60 (2010).

18. Jung, Y. S., Chang, J. B., Verploegen, E., Berggren, K. K. & Ross, C. a. A path to ultranarrow patterns using self-assembled lithography. *Nano Lett.* **10,** 1000–5 (2010).

19. Kim, B. H. *et al.* Wrinkle-directed self-assembly of block copolymers for aligning of nanowire arrays. *Adv. Mater.* **26,** 4665–70 (2014).

20. Cheng, J. Y., Rettner, C. T., Sanders, D. P., Kim, H.-C. & Hinsberg, W. D. Dense Self-Assembly on Sparse Chemical Patterns: Rectifying and Multiplying Lithographic Patterns Using Block Copolymers. *Adv. Mater.* **20,** 3155–3158 (2008).

21. Stoykovich, M. P. *et al.* Directed assembly of block copolymer blends into nonregular device-oriented structures. *Science* **308,** 1442–6 (2005).

22. Cheng, J. Y., Ross, C. a., Thomas, E. L., Smith, H. I. & Vancso, G. J. Fabrication of nanostructures with long-range order using block copolymer lithography. *Appl. Phys. Lett.* **81,** 3657 (2002).

23. Cheng, J. Y., Mayes, A. M. & Ross, C. a. Nanostructure engineering by templated self-assembly of block copolymers. *Nat. Mater.* **3,** 823–8 (2004).

24. Jung, Y. S. & Ross, C. a. Orientation-controlled self-assembled nanolithography using a polystyrene-polydimethylsiloxane block copolymer. *Nano Lett.* **7,** 2046–50 (2007).

25. Chang, J.-B. *et al.* Design rules for self-assembled block copolymer patterns using tiled templates. *Nat. Commun.* **5,** 3305 (2014).

26. Tavakkoli K G, a *et al.* Templating three-dimensional self-assembled structures in bilayer block copolymer films. *Science* **336,** 1294–8 (2012).

27. Tavakkoli, A. K. G. *et al.* Sacrificial-post templating method for block copolymer self-assembly. *Small* **10,** 493–9, 418 (2014).

28. Cord, B. *et al.* Limiting factors in sub-10 nm scanning-electron-beam lithography. *J. Vac. Sci. Technol. B Microelectron. Nanom. Struct.* **27,** 2616 (2009).

29. Manfrinato, V. R. *et al.* Resolution limits of electron-beam lithography toward the atomic scale. *Nano Lett.* **13,** 1555–8 (2013).

30. Yang, J. K. W. J. & Berggren, K. K. Using high-contrast salty development of hydrogen silsesquioxane for sub-10-nm half-pitch lithography. *J. Vac. Sci. Technol. B Microelectron. Nanom. Struct.* **25,** 2025 (2007).

31. Yang, J. K. W. *et al.* Understanding of hydrogen silsesquioxane electron resist for sub-5-nm-half-pitch lithography. *J. Vac. Sci. Technol. B Microelectron. Nanom. Struct.* **27,** 2622 (2009).

32. Duan, H. *et al.* Metrology for electron-beam lithography and resist contrast at the sub-10 nm scale. *J. Vac. Sci. Technol. B Microelectron. Nanom. Struct.* **28,** C6H11 (2010).

33. Tavakkoli K G, A. *et al.* Rectangular symmetry morphologies in a topographically templated block copolymer. *Adv. Mater.* **24,** 4249–54 (2012).

34. Do, H. W., Chang, J.-B. & Berggren, K. K. Three-dimensional nanofabrication using hydrogen silsesquioxane/poly(methylmethacrylate) bilayer resists. *J. Vac. Sci. Technol. B, Nanotechnol. Microelectron. Mater. Process. Meas. Phenom.* **32,** 06F501 (2014).

35. Duan, H. *et al.* Sub-10-nm half-pitch electron-beam lithography by using poly(methyl methacrylate) as a negative resist. *J. Vac. Sci. Technol. B Microelectron. Nanom. Struct.* **28,** C6C58 (2010).

36. Wu, N. L. Y., Harris, K. D. & Buriak, J. M. Conversion of bilayers of PS-b-PDMS block copolymer into closely packed, aligned silica nanopatterns. *ACS Nano* **7,** 5595–606 (2013).

37. Cui, B., Yu, Z., Ge, H. & Chou, S. Y. Large area 50 nm period grating by multiple nanoimprint lithography and spatial frequency doubling. *Appl. Phys. Lett.* **90,** 043118 (2007).

38. Chen, Y. *et al.* Spatial frequency multiplication techniques towards half-pitch 10nm patterning. in *SPIE 7973, Opt. Microlithogr. XXIV* (Dusa, M. V.) **7973,** 79731T–79731T-7 (2011).

39. Chang, T. Proximity Effect in Electron-beam Lithography. *J. Vac. Sci. Technol.* (1975). at <http://scitation.aip.org/content/avs/journal/jvst/12/6/10.1116/1.568515>

40. Gotrik, K. W. & Ross, C. a. Solvothermal annealing of block copolymer thin films. *Nano Lett.* **13,** 5117–22 (2013).

41. Lille, J. *et al.* Imprint lithography template technology for bit patterned media (BPM). in *SPIE 8166, Photomask Technol.* (Maurer, W. & Abboud, F. E.) **8166,** 816626 (2011).

42. Herr, D. J. C. Directed block copolymer self-assembly for nanoelectronics fabrication. *J. Mater. Res.* **26,** 122–139 (2011).

43. Patel, K. C. *et al.* Line-frequency doubling of directed self-assembly patterns for single-digit bit pattern media lithography. **8323,** 83230U–83230U-9 (2012).

44. Wu, N. L. Y. *et al.* Density doubling of block copolymer templated features. *Nano Lett.* **12,** 264–8 (2012).

45. Park, W. I. *et al.* Host-guest self-assembly in block copolymer blends. *Sci. Rep.* **3,** 3190 (2013).

46. Duan, H. & Berggren, K. K. Directed self-assembly at the 10 nm scale by using capillary force-induced nanocohesion. *Nano Lett.* **10,** 3710–6 (2010).

47. Duan, H., Yang, J. K. W. & Berggren, K. K. Controlled collapse of high-aspect-ratio nanostructures. *Small* **7,** 2661–8 (2011).